

OBSERVATIONAL CONSTRAINTS ON THE CO-EVOLUTION OF SUPERMASSIVE BLACK HOLES AND GALAXIES

X. Z. ZHENG,¹ E. F. BELL,^{2,3} R. S. SOMERVILLE,^{2,4} H.-W. RIX,² K. JAHNKE,² F. FONTANOT,^{2,5} G. H. RIEKE,⁶ D. SCHIMINOVICH,⁷ K. MEISENHEIMER²

Accepted by ApJ

ABSTRACT

The star formation rate (SFR) and black hole accretion rate (BHAR) functions are measured to be proportional to each other at $z \lesssim 3$. This close correspondence between SF and BHA would naturally yield a BH mass–galaxy mass correlation, whereas a BH mass–bulge mass correlation is observed. To explore this apparent contradiction we study the SF in spheroid-dominated galaxies between $z = 1$ and the present day. We use 903 galaxies from the COMBO-17 survey with $M_* > 2 \times 10^{10} M_\odot$, ultraviolet and infrared-derived SFRs from Spitzer and GALEX, and morphologies from GEMS HST/ACS imaging. Using stacking techniques, we find that <25% of all SF occurs in spheroid-dominated galaxies (Sérsic index $n > 2.5$), while the BHAR that we would expect if the global scalings held is three times higher. This rules out the simplest picture of co-evolution, in which SF and BHA trace each other at all times. These results could be explained if SF and BHA occur in the same events, but offset in time, for example at different stages of a merger event. However, one would then expect to see the corresponding star formation activity in early-stage mergers, in conflict with observations. We conclude that the major episodes of SF and BHA occur in different events, with the bulk of SF happening in isolated disks and most BHA occurring in major mergers. The apparent global co-evolution results from the regulation of the BH growth by the potential well of the galactic spheroid, which includes a major contribution from disrupted disk stars.

Subject headings: galaxies: evolution — galaxies: active – quasars: general

1. INTRODUCTION

The last decade has seen the discovery and characterization of an unexpectedly tight correlation between the mass of supermassive black holes (SMBH; M_{BH}) and the mass (M_{bulge}) or velocity dispersion of their host galaxy’s bulge (Magorrian et al. 1998; Ferrarese & Merritt 2000; Gebhardt et al. 2000; Marconi & Hunt 2003; Häring & Rix 2004). The black hole mass appears to be most strongly correlated with the bulge mass, not the total mass (Kormendy 2001; Ho 2007); the scatter in this relation between bulge mass and black hole mass is estimated to be less than a factor of two (Häring & Rix 2004).

This relationship indicates that galaxy and black hole formation and evolution are interconnected.⁸ In its weak form, such an interconnection could result if the black hole growth is limited by the wider galaxy environment (‘dog wagging the tail’). Stronger forms of interconnection are also possible. The energy released by a growing SMBH is sufficient, if it couples effectively with its surroundings, to have dra-

matic consequences on the galaxy (‘tail wagging the dog’). For example, the injection of energy into hot halo gas in galaxy clusters is indicated by the inflation of bubbles and the propagation of sound waves (McNamara et al. 2000, 2005; Fabian et al. 2003; Rafferty et al. 2006). Furthermore, it is possible that SMBHs with high accretion rates drive powerful outflows that remove (at least some) cold gas from galaxies (Chartas et al. 2003; Crenshaw et al. 2003; Pounds et al. 2003; Tremonti et al. 2007). In fact, feedback from an accreting SMBH/AGN may help address many of the most difficult issues affecting models of galaxy evolution in a cosmological context: e.g., overcooling in massive halos and late star formation in elliptical galaxies (Binney & Tabor 1995; Croton et al. 2006; Bower et al. 2006; Monaco et al. 2007; Somerville et al. 2008).

A diversity of models has been constructed to explore the interrelationship between bulge mass and black hole mass, featuring both weak and strong aspects of the possible interconnections (Somerville et al. 2008, and references therein). However, the details of the physical processes governing BH formation and growth, and the physical mechanisms whereby SMBHs couple with their host galaxies and surroundings remain poorly understood. It will be impossible to model the full range of interconnected processes from theoretical first principles for some time, as the physics of the formation of SMBHs and galaxy evolution spans at least ≈ 7 orders of magnitude in scale. Empirical and phenomenological constraints are therefore extremely important.

A common feature of most “unified” models of SMBH and galaxy formation is the concept of co-evolution, whereby the SMBHs and their galaxies evolve under each other’s influence. The term co-evolution means many things to many people (e.g., Silk & Rees 1998; Kauffmann & Haehnelt 2000; Wyithe & Loeb 2003; Granato et al. 2004; Merloni et al. 2004; Haiman, Ciotti & Ostriker 2004; Cattaneo et al. 2005; Fontanot et al. 2006). For the purpose of having strawmen to

¹ Purple Mountain Observatory, Chinese Academy of Sciences, West Beijing Road 2, Nanjing 210008, China; xzzheng@pmo.ac.cn

² Max-Planck Institut für Astronomie, Königstuhl 17, D-69117 Heidelberg, Germany

³ University of Michigan, 500 Church St., Ann Arbor, MI 48109

⁴ Space Telescope Science Institute, 3700 San Martin Drive, Baltimore, MD 21218

⁵ INAF-Osservatorio Astronomico, Via Tiepolo 11, I-34131 Trieste, Italy

⁶ Steward Observatory, University of Arizona, 933 N Cherry Ave, Tucson, AZ 85721

⁷ Department of Astronomy, Columbia University, New York, NY 10027

⁸ Peng (2007), noting that multiple generations of mergers would reduce the scatter of a weak or non-existent $M_{\text{bulge}} - M_{\text{BH}}$ relation essentially through the central limit theorem, found that more than 10 generations of major mergers would be required to imprint a tight $M_{\text{bulge}} - M_{\text{BH}}$ relation in a population that was initially uncorrelated. Such a large number of major mergers is highly unlikely, arguing that while mergers may tighten this relation much of the correlation must be imprinted through a strong interconnection between M_{bulge} and M_{BH} .

take aim at, we outline three possible scenarios:

- **Strong Co-evolution:** In its strongest sense, co-evolution implies that bulges and black holes grow *together*, i.e., in the same objects and at the same time. In this case, BH growth could be thought of as a sort of a ‘tax’: whenever star formation occurs, the SMBH accretes some fraction of the mass involved. This scenario in its simplest form can already be ruled out — there are many examples of star-forming bulges without AGN activity and bulges with AGN activity and no SF (e.g., M87).
- **Time Offset:** One could imagine a scenario in which bulge stars and SMBHs are formed in the same event, but on different timescales and/or stages of the event. For example, star formation might occur predominantly in the early stages of a merger, while BH growth might occur in the later stages (e.g., Di Matteo et al. 2005; Hopkins et al. 2005, 2006). Such a picture would predict little evolution in the BH-bulge mass correlation for an unbiased ensemble, but galaxies in the throes of their bulge building events (or black holes in their most rapid growth phase) could exhibit significant deviations from the scaling relations; this hypothesis is considerably more challenging to rule out.
- **Regulated Growth:** A third possibility is that the major episodes of SF and BH accretion occur in different events, but the growth of one component regulates that of the other. For example, if black hole growth is regulated by feedback from the AGN itself, as suggested by many workers (e.g., Silk & Rees 1998; Murray, Quataert & Thompson 2005; Di Matteo et al. 2005), the potential well of the pre-existing bulge determines how much energy is needed to stop further accretion and halt the growth of the black hole, and hence the final black hole mass. It is possible, even likely, that the bulge stars that dominate this potential well are formed mostly in previous star formation “events”, i.e. in progenitor disks which have subsequently merged. In this picture, one would expect a larger possible disconnect between observable episodes of SF vs. BH accretion *activity*, even while the endpoints of this activity (bulges and black holes) are expected to end up being tightly related.

There are a number of ways to attack the problem of co-evolution observationally. Obviously, measuring the BH-bulge mass correlation at the present day at extremely low or high mass will provide powerful insights into the processes linking galaxy and SMBH evolution (Barth et al. 2005; Lauer et al. 2007a). The study of the BH-bulge mass correlation during BH or bulge-building events is also an important avenue of approach (e.g., Barth et al. 2005; Greene & Ho 2006; Treu et al. 2004, 2007; Woo et al. 2006; Peng et al. 2006; Borys et al. 2005). The most commonly-used technique in the latter approach is studying the masses of actively-accreting Type I AGN for which BH masses can be estimated using an empirically-calibrated combination of luminosity and broad line region line width (Wandel, Peterson & Malkan 1999; Baskin & Laor 2005; Kaspi et al. 2005; Vestergaard & Peterson 2006, and references therein); current results are controversial but tentatively support larger BH to bulge mass ratios at early

times than those seen today (Treu et al. 2004; Woo et al. 2006; Peng et al. 2006; Shields et al. 2006, see also, e.g., Alexander et al. 2005 for the smaller ratios of black hole to bulge mass in rapidly-star-forming galaxies detected in the submm).

With current generations of wide and deep cosmological surveys, another means has opened up: comparison of evolution of the BH accretion rate (BHAR) and that of the SFR of galaxies (Silverman et al. 2009; see Boyle & Terlevich 1998 and Franceschini et al. 1999, for early efforts). The history of BH accretion has been explored using primarily optical and X-ray techniques, with important insights being gained from observations in the radio and infrared (Miyaji, Hasinger & Schmidt 2000; Ueda et al. 2003; Hasinger, Miyaji & Schmidt 2005; La Franca et al. 2005; Barger et al. 2005; Donley et al. 2005; Brown et al. 2006; Richards et al. 2006a). Furthermore, a decade of intensive multi-wavelength and redshift surveying has placed powerful and interesting constraints on the volume-averaged SF history of the Universe (Hopkins & Beacom 2006; Pérez-González et al. 2005; Le Floch et al. 2005; Schiminovich et al. 2005). In both cases, the integrated BH accretion and SF histories give values that match to within a factor of 2 or 3 of the present-day BH mass and stellar mass⁹ densities (Yu & Tremaine 2002; Marconi et al. 2004; Borch et al. 2006; Fardal et al. 2007; Wilkins et al. 2008); we will discuss in detail uncertainties and possible inconsistencies between the integral of the SFR and the present-day stellar mass in §2.

The observational maturity of current datasets at $z < 1$ allows the use of a novel angle of attack on the problem of co-evolution. Recent multi-wavelength/HST surveys have covered enough volume that SFR density and BHAR density can be estimated in well-defined subsamples of galaxies for the first time, offering potentially decisive insight into not only the statistical evolution of these quantities, but into whether black holes and bulges are actually growing *in the same objects and at the same time*. This is the approach we will adopt in this paper. To do this, we first examine the global SFR and BHAR (§2), then the multiplicity functions¹⁰ of SFR and BHAR as a function of redshift (§3). In §4, we present new measurements of SF activity in mass and morphology-limited samples of galaxies, and examine accretion activity driven by massive BHs in massive spheroids under assumptions widely used in literature. In §5, we discuss the results in the context of co-evolution and summarize our conclusions. Throughout the paper we assume a cosmology with $H_0 = 70 \text{ km s}^{-1} \text{ Mpc}^{-1}$, $\Omega_M = 0.3$ and $\Omega_\Lambda = 0.7$.

2. THE COSMIC STAR FORMATION AND BH ACCRETION HISTORIES

We first attempt to give some context to the analysis that will follow by exploring the cosmic star formation and black hole accretion histories.

2.1. The cosmic star formation history

During the last decade, a number of studies have contributed to determining the average SFR per co-moving vol-

⁹ In the case of stellar mass density, recycling of nearly 1/2 of the initial stellar mass back into interstellar gas must be accounted for to avoid dramatically overproducing the present-day stellar mass density.

¹⁰ The comoving number density of sources with a given SFR or BHAR — e.g., a luminosity function is a multiplicity function

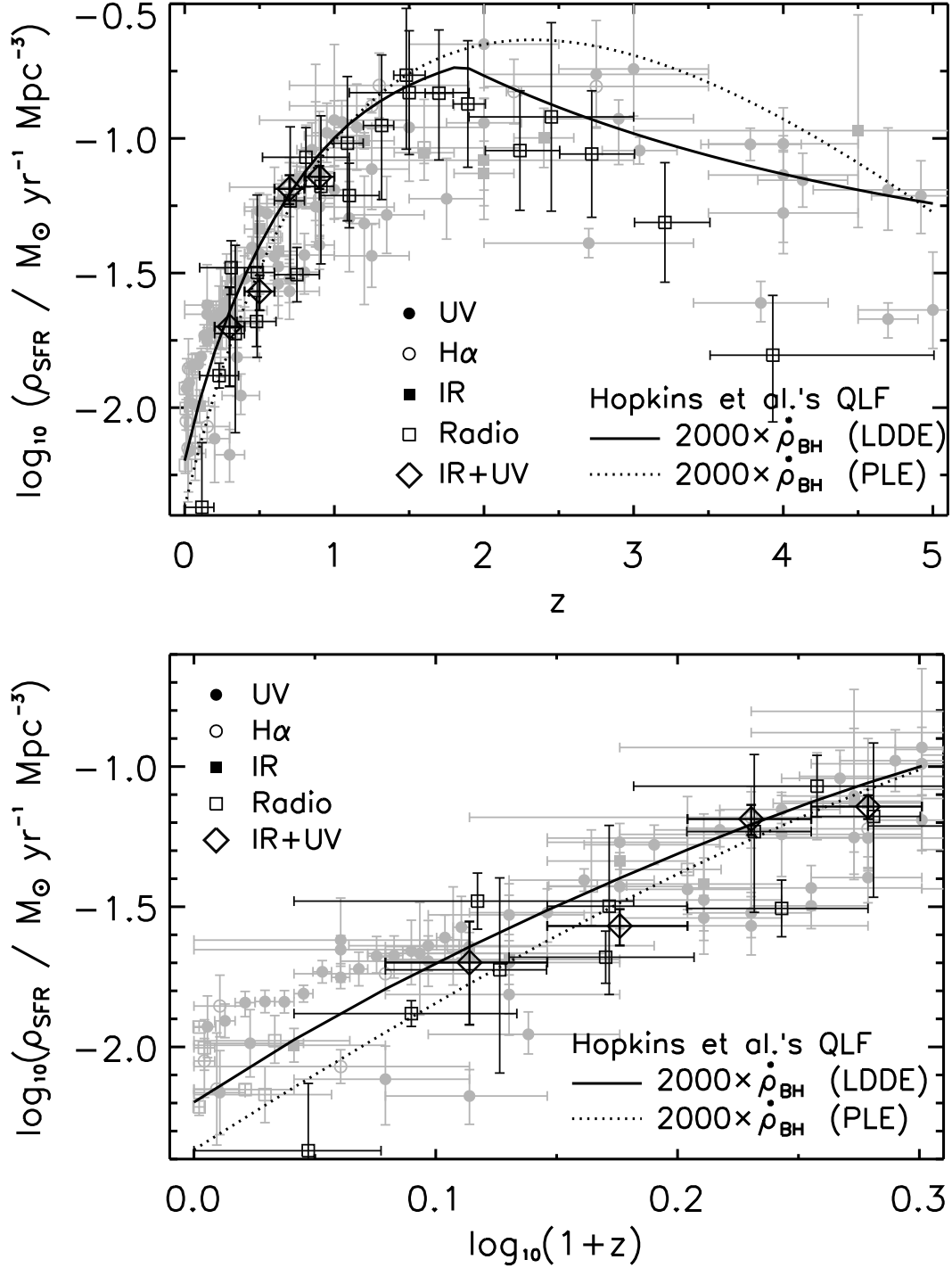


FIG. 1.— *Top*: Comparison between the volume-averaged SF history and the volume-averaged BH accretion history; *Bottom*: The same comparison but only in the redshift range $0 < z < 1$. The *gray* data points come from the compilation of available measurements by Hopkins & Beacom (2006). The *black squares* are radio measurements from Seymour et al. (2008), Smolčić et al. (2009) and Dunne et al. (2008). The *black diamonds* represent IR+UV measurements from Bell et al. (2007). All measurements are converted to a Kroupa IMF and the same cosmology adopted here. The BH accretion history is derived from AGN bolometric luminosity functions given in HRH07 by assuming a radiation efficiency $\epsilon = 0.1$. The BH accretion history is shifted upwards by 3.3 dex (a factor of 2000).

ume at different cosmic epochs with various SFR estimators (e.g., UV, H α , IR and radio). The available measurements from the literature compiled by Hopkins & Beacom (2006), and complemented with recent measurements from Seymour et al. (2008), Smolčić et al. (2009) and Dunne et al. (2008) are shown in Figure 1. We include also recent estimates from the use of UV and 24 μ m data to account for both unobscured and obscured star formation at $z < 1$ (Zheng et al. 2007; Bell et al. 2007). Here all measurements are corrected to our adopted cosmology and a Kroupa (2001) initial mass function (IMF). It can be seen from Figure 1 that the cosmic SFR density increases rapidly with redshift, peaks at $z \sim 1.5$, then becomes flat or declines at $z > 1.5$, although the uncertainties are large at these early epochs. The cosmic SFR density decreases by an order of magnitude from the $z = 1$ to the present day, following $\rho_{\text{SFR}} \sim (1+z)^{2.9 \pm 0.2}$.

A complementary measurement to the cosmic SFR density is the cosmic stellar mass density. The assembly of stellar mass should be consistent with the integral of the cosmic SFR density. Current measurements show a reasonably good agreement between the two, at least at redshifts less than about unity (Borch et al. 2006; Bell et al. 2007; Wilkins et al. 2008); about 40-50% of local stars were formed since $z = 1$ (Dickinson et al. 2003; Fontana et al. 2003; Drory et al. 2005; Borch et al. 2006; Rudnick et al. 2006). As an aside, it is worth noting that there is a possible mismatch between the integral of the cosmic SFR density at $z > 1$ with the stellar mass observed to be in place at $z = 1$: it appears that the integral is a factor of ~ 3 in excess of the stellar mass formed by $z = 1$. The origin of this mismatch is currently not well-understood. It is possible that this discrepancy signals a break-down in the utility of SFR indicators or a change or break-down of a universally-applicable stellar IMF. It should also be noted that at $z > 1$ the estimates of SFR (and stellar mass) are highly uncertain; in particular, the relatively sensitive UV measurements need to be corrected for substantial (factors of a few) dust extinction using defensible but uncertain recipes (Reddy et al. 2008), and measurements of the rest-frame IR and radio probe only the most luminous systems (see, e.g., Dunne et al. 2008 for substantial progress towards this goal using stacking of radio data; it is interesting that their resulting SFR densities are much lower than those reported previously at $z \geq 1.5$). Yet, for our purposes, the possibility of a mismatch between SFR and stellar mass at $z > 1$ is of relatively little importance; the focus of our work is at the better-constrained $z < 1$ redshift range.

2.2. The cosmic BH accretion history

Observed (optically “bright”) BH accretion apparently can account for nearly all of the BH mass seen in remnants today, indicating that the bulk of BH mass growth occurs during a luminous AGN phase with a radiation efficiency $\epsilon \sim 0.1$ (e.g., Yu & Tremaine 2002; Marconi et al. 2004; Shankar et al. 2004). The observed AGN luminosity function is therefore a reasonable probe of the cosmic BH accretion history. From deep cosmological surveys performed with modern observational facilities, AGN luminosity functions have been determined out to $z \sim 4$ in hard X-ray (e.g., Ueda et al. 2003; La Franca et al. 2005; Barger et al. 2005), soft X-ray (e.g., Miyaji, Hasinger & Schmidt 2000; Hasinger, Miyaji & Schmidt 2005), optical (e.g., Croom et al. 2004; Richards et al. 2006b; Fontanot et al. 2007) and mid-IR bands (e.g., Brown et al. 2006; Richards et al. 2006a). The intrinsic spectral energy distribution (SED) of AGN is thought

to be only a function of luminosity (e.g., Marconi et al. 2004); and accounting for obscuration, the AGN luminosity functions of different bands are correlated through the SED. Hopkins et al. (2007b, hereafter HRH07) presented bolometric AGN LFs derived from the combination of AGN LFs measured in multi-wavelength bands, from mid-IR through hard X-ray (see their paper and references therein for details of the AGN LFs and related uncertainties). We caution that Compton-thick AGN are not counted in the HRH07 bolometric LFs. Correction for the missing accretion is suggested to be ≤ 0.15 dex (a factor of 1.4; see HRH07 for more discussion). HRH07 presented several evolution models which fit the AGN bolometric luminosity function at different cosmic epochs. We adopted the best-fit pure luminosity evolution (PLE) model and the luminosity-dependent density evolution (LDDE) model of the bolometric LF $\Phi(L_{\text{bol}}, z)$ from HRH07 to calculate the BHAR per co-moving volume as follows:

$$\dot{\rho}_{\text{BH}}(z) = \int_0^\infty \frac{(1-\epsilon)L_{\text{bol}}}{\epsilon c^2} \Phi(L_{\text{bol}}, z) dL_{\text{bol}}, \quad (1)$$

where L_{bol} is the bolometric luminosity and we have adopted $\epsilon = 0.1$. By default L_{bol} is given in units of erg s^{-1} . We integrate the bolometric luminosity over the range $43 < \log L_{\text{bol}} < 49$. The cosmic BHAR density peaks at $z \sim 1.9$, and dramatically decreases to the present day. At $z > 1.9$, the cosmic BHAR density is likely to decline or stay flat to earlier cosmic times although the uncertainties are large (see also Barger et al. 2005). Roughly speaking, the cosmic BHAR density increases as $\dot{\rho}_{\text{BH}} \sim (1+z)^\alpha$ and $\alpha \sim 3.4$ up to $z = 1$. Considering the uncertainties of different band LFs and uncertainties in bolometric correction, a typical error of ~ 0.6 is adopted for the power index α .

2.3. Comparison between the cosmic star formation and BH accretion histories

Figure 1 shows the cosmic SFR density to be in good agreement with the cosmic BHAR density scaled by a factor of 2000 over a wide redshift range from $z \sim 0$ to $z \sim 5$. The factor 2000 is the ratio of the integral of the cosmic SFR density to the integral of the cosmic BHAR density within the redshift range from $z = 0$ to $z = 1$, where both quantities are well determined. In the redshift range $0 < z < 1$ a quantitative comparison between the cosmic SFR density and BHAR density can be made: they increase with redshift with almost the same slope of $\dot{\rho} \sim (1+z)^3$ within the errors. Figure 1 suggests that the cosmic BH accretion history is parallel to the cosmic SF history.

If the strong co-evolution hypothesis is correct, the shift between the volume-averaged SFR and volume-averaged BHAR (a factor of 2000; 3.3 dex) should be consistent with the difference between the local stellar mass density and BH mass density. The integral of the SFR needs to be corrected for the recycling of mass back into gas during the process of stellar evolution; with our adopted IMF, almost 50% of the initially-formed stellar mass is returned to the ISM within 5–7 Gyr. Thus, one expects a ratio of local stellar mass density to BH mass density of ~ 1000 . This is consistent with the measurements of local stellar mass density $\rho_{*,0} = 3.0^{+0.8}_{-0.6} \times 10^8 \text{ M}_\odot \text{ Mpc}^{-3}$ (e.g., Bell et al. 2003) and local BH mass density $\rho_{\text{BH},0} = 4.6^{+1.9}_{-1.4} \times 10^5 \text{ M}_\odot \text{ Mpc}^{-3}$ (e.g., Marconi et al. 2004).

Thus, somewhat remarkably, it appears that the histories of SMBH accretion and star formation are very similar in shape,

TABLE 1
BEST-FIT PARAMETERS FOR THE SFR
FUNCTIONS.^a

z_{start}	z_{end}	$\log SFR^*$ ($M_{\odot} \text{ yr}^{-1}$)	$\log \Phi^*$ ($\text{Mpc}^{-3} \text{ dex}^{-1}$)
0.2	0.4	1.09	-2.80
0.4	0.6	1.11	-2.77
0.6	0.8	1.12	-2.63
0.8	1.0	1.15	-2.90

^a The SFR functions are given in the form of “double power-law”, $\log \Phi = \log \Phi^* + \alpha \log SFR$, with $\alpha = -0.6$ and $\alpha = -2.2$ for SFR below and above SFR^* , respectively.

offset by a ratio consistent with the ratio between BH mass and stellar mass density at the present day. Put differently, it appears that the ratio of stellar mass to SMBH mass density is *independent* of redshift, in seeming accord with the co-evolution picture.

3. STATISTICAL LINKS BETWEEN SF AND BH ACCRETION EVENTS

The overall BH accretion/SF mass ratio results from the sum of individual BH accretion/SF events in the same cosmic epoch. Here, a BH accretion “event” means a SMBH in the active phase (i.e., AGN) and a SF event refers to a galaxy of a given SFR. In this section we address whether the intensity of star formation events is statistically correlated with the intensity of BH accretion events.

Following the description in §2.2, we convert the AGN bolometric luminosity functions of HRH07 into BHAR functions by assuming $\epsilon = 0.1$. We take the BHAR functions described by a double power-law as describing the statistics of BH accretion events. Bell et al. (2007) estimated the SFR using bolometric (UV+IR) luminosity for a sample of 7506 galaxies and derived SFR functions in four redshift slices between $z = 0.2$ and $z = 1$. Motivated by local IR luminosity functions that are well-fit with a “double power-law” shape (Sanders et al. 2003, having a form of $\Phi(L) \propto L^{\alpha}$ with $\alpha = -0.6(\pm 0.1)$ and $\alpha = -2.2(\pm 0.1)$ for $L < L^*$ and $L > L^*$, respectively), we re-fit the SFR functions of Bell et al. (2007) with a double power-law. The best-fit parameters for these SFR functions are given in Table 1. We adopt these SFR multiplicity functions to describe the statistics of SF events.

Figure 2 shows the adopted BHAR functions and SFR functions. We have shown in §2.3 that the cosmic BH accretion history tracks the cosmic SF history through a universal scaling factor of 2000. Comparing the BHAR function with the SFR function, we find that the former always tracks the latter in all four redshift slices from $z = 0.2$ to $z = 1$ after being re-scaled by a factor of 20 in BHAR and by 100 in number density, as shown in Figure 2. The two scaling factors 20 and 100 are empirically determined to make the agreement between the two functions as good as possible, particularly in the wide regime around the SFR function “knee” (i.e., $0 < \log(SFR/M_{\odot} \text{ yr}^{-1}) < 2$), where the vast majority of the total SF occurs. We split SF events by their intensity into three classes: high-intensity ($SFR > 100 M_{\odot} \text{ yr}^{-1}$; i.e., ultraluminous IR galaxies), medium-intensity ($10 < SFR < 100 M_{\odot} \text{ yr}^{-1}$; i.e., luminous IR galaxies) and low-intensity ($SFR < 10 M_{\odot} \text{ yr}^{-1}$; i.e., “normal” galaxies). Similarly, we split BH accretion events into the same three classes by replacing SFR with $20 \times BHAR$. The three classes

of AGN roughly correspond to luminous quasars, quasars and Seyferts/low-luminosity AGN, respectively. From the adopted SFR/BHAR functions, we calculate the volume-averaged SFRs/BHARs contributed by the three classes, respectively. The results are shown in Figure 3.

As can be seen from Figure 3, the volume-averaged SFR/BHAR contained in high-intensity star formation or BH accretion events decreases dramatically from $z = 1$ to $z = 0.2$, whereas the decrease of the volume-averaged SFR/BHAR with decreasing redshift is gradually slower for the medium-intensity and low-intensity SF and BH accretion events. The low-intensity SF and BH accretion events dominate the cosmic SFR/BHAR at low- z and the high-intensity star formation/BH accretion events start to dominate the cosmic SFR/BHAR at $z > 0.8$. It is clear that for either the medium-intensity or the low-intensity class, the volume-averaged SFR matches the volume-averaged BHAR remarkably well over the redshift range $0.2 < z < 1$. For the high-intensity class, the agreement is poor, possibly because of the large uncertainties in the SFR and BHAR functions in this range ($SFR > 100 M_{\odot} \text{ yr}^{-1}$ or $20 \times BHAR > 100 M_{\odot} \text{ yr}^{-1}$). We conclude that SF events statistically track BH accretion events over $0.2 < z < 1$ when split by intensity.

4. CHARACTERIZING THE HOST GALAXIES OF STAR FORMATION AND BH ACCRETION

In §2 and §3, we presented evidence that both the distribution (multiplicity functions) and integrals of the SF rate and supermassive black hole accretion rate evolve similarly at all redshifts, with an offset in integrated rate of a factor of ~ 2000 at all $z \lesssim 1$. Taken at face value, such a coincidence may lead one to predict a correlation between galaxy mass and supermassive black hole mass, offset by a factor of ~ 1000 in zero point (where the expected offset is a factor of 1000 rather than 2000 because of the recycling of stellar mass during the course of stellar evolution). Such a correlation is not observed; instead, it appears that *bulge* mass and supermassive black hole mass correlate (Kormendy 2001).

In this section, we present new measurements of the relationship between SFR and BHAR for spheroid-dominated galaxies, in order to investigate the seeming disconnect between a BH-bulge mass relation on one hand, and the close correspondence between SFR and BHAR statistics on the other.

4.1. Links between SFR, stellar mass and morphology

4.1.1. The data

We address this issue using a deep, wide-area multi-wavelength dataset from the extended Chandra Deep Field South (ECDFS). We use optical photometry, photometric redshift catalogs ($\delta z/(1+z) \sim 0.02$; Wolf et al. 2004) and stellar mass estimates (Borch et al. 2006) from the COMBO-17 survey for ~ 9000 galaxies with aperture magnitudes $m_R < 23.5$ mag and $z < 1.1$ in the $30'5 \times 30'$ ECDFS. High-resolution (0'07) HST imaging from the Galaxy Evolution from Morphology and SEDs (GEMS) survey (Rix et al. 2004) covers around 800 square arcminutes of the ECDFS in the F606W and F850LP passbands, providing optical morphologies for ~ 8000 galaxies. A two-dimensional light distribution analysis is performed on the F850LP imaging data using the software tool GALFIT, providing Sérsic index n as a broad measure of

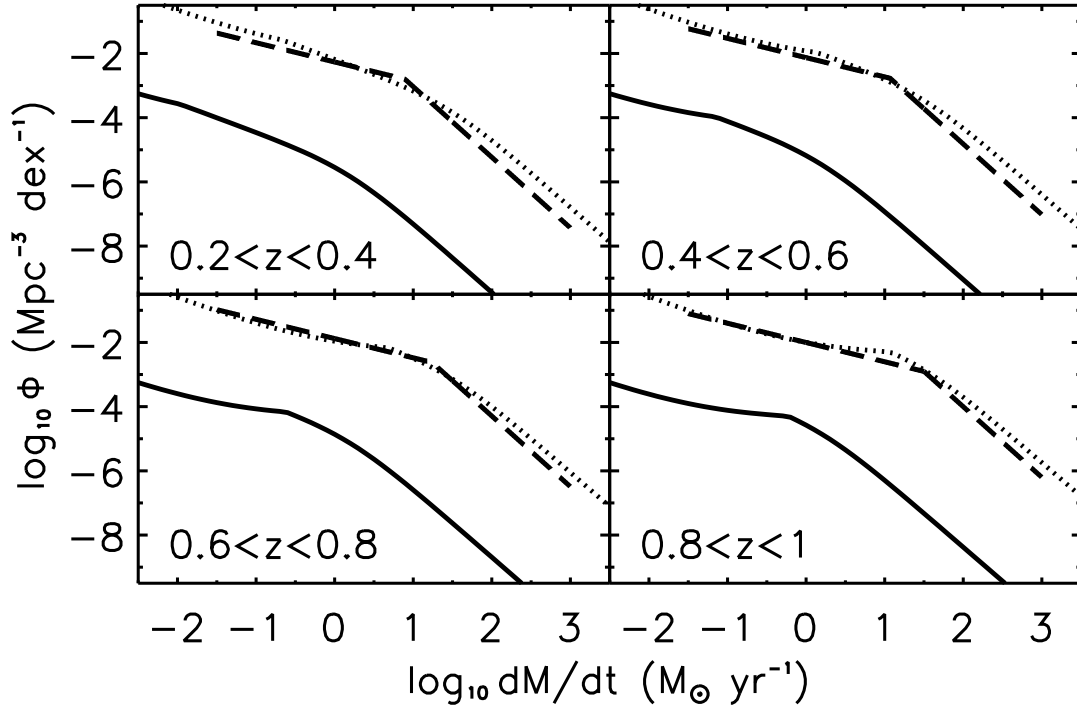


FIG. 2.— Comparison between the SFR functions (the *dashed* lines) and the BHAR functions (the *solid* lines) in four redshift bins from $z = 0.2$ to $z = 1$. The SFR functions are obtained by fitting the data points in Bell et al. (2007) with “double power-law” function from Sanders et al. (2003, see text for details). The BHAR function is the conversion of the AGN bolometric luminosity function from HRH07 with a radiation efficiency $\epsilon = 0.1$. The *dotted* lines are the BHAR functions shifted by 20 along the x-axis and 100 along the y-axis.

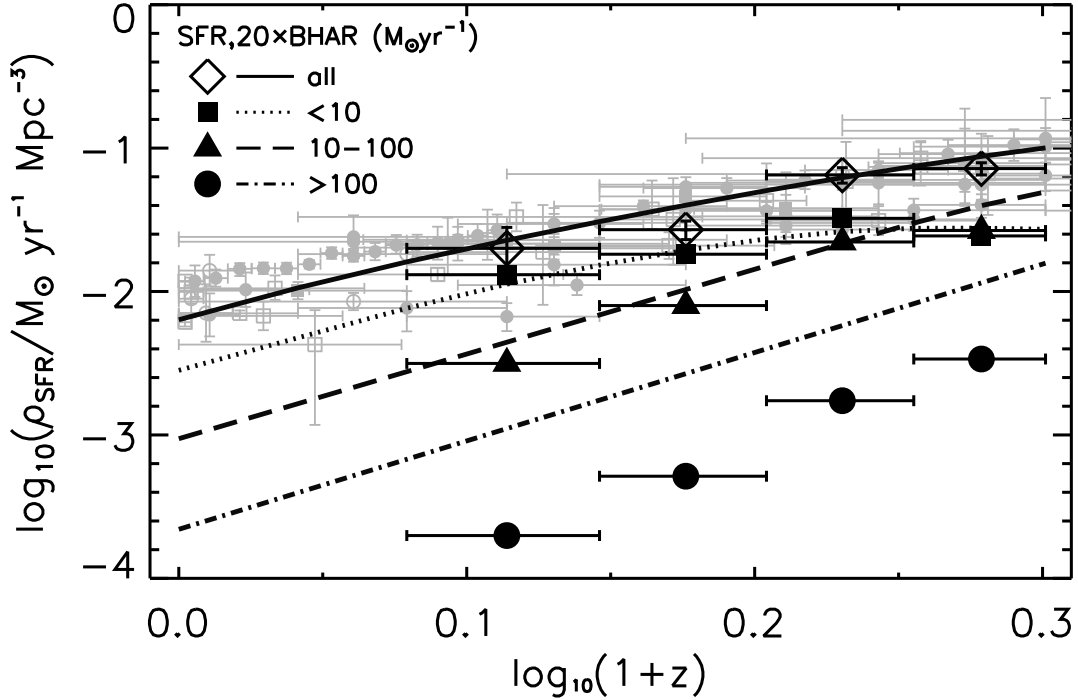


FIG. 3.— The cosmic SFR density (solid symbols) and BHAR density (lines) split into high-intensity (circles; the *dot-dashed* line), medium-intensity (triangles; the *dashed* lines) and low-intensity episodes (squares; the *dotted* lines).

the concentration of a galaxy (Häußler et al. 2007).¹¹

Deep far-ultraviolet (FUV; 1350-1750Å) and near-ultraviolet (NUV; 1750-2800Å) images centered on the ECDFS were obtained by the *Galaxy Evolution Explorer* (GALEX; Martin et al. 2005), with a field of view of a square degree. The FUV and NUV images have a typical resolution $\sim 5''$, and a depth of $3.63 \mu\text{Jy}$ at the 5σ detection level. Data reduction and source detection is described in Morrissey et al. (2005). Deep $24 \mu\text{m}$ data of the ECDFS were taken as part of the MIPS GTO observations (Rieke et al. 2004). A mosaic image was produced with a rectangular field of $90' \times 30'$. The $24 \mu\text{m}$ image has a point spread function (PSF) with full width at half maximum (FWHM) $\approx 6''$. Sources are detected down to $83 \mu\text{Jy}$ at the 5σ level (see Papovich et al. 2004, for details of data reduction, source detection and photometry).

4.1.2. Sample selection

The goal of §4 is to study the SFR in massive galaxies split by morphology (or, more precisely, structure, as we use Sérsic index n to differentiate between spheroid- and disk-dominated galaxies). Accordingly, in this section, we define the mass-limited, SFR-limited and structurally (morphologically)-selected galaxy samples that we use for further study.

A sample of 903 massive galaxies ($M_* \geq 2 \times 10^{10} M_\odot$) in the redshift range of $0.2 < z < 1$ is selected from the COMBO-17/GEMS survey in the ECDFS. These objects are located in the overlap area (~ 600 square arcminutes) of the *HST*, *GALEX* and MIPS observations that allow for SFR measurements. We have removed X-ray point sources detected in the Chandra 250 ks observation (Lehmer et al. 2005) in order to exclude AGN-heated dust and AGN UV emission (we describe later how this selection criterion is of only modest importance; less than 15% of star formation is in such systems). For the present comparison, we identify spheroid-dominated galaxies with galaxies of Sérsic index $n > 2.5$. The criterion $n = 2.5$ is a reasonable and reproducible separation between concentrated early-type galaxies and late-type galaxies (Bell et al. 2004b; Pannella et al. 2006, see, e.g., van der Wel et al. 2008 for a discussion of the relationship between morphology and Sérsic index in the SDSS). In what follows, we use this 903-galaxy sample to define three galaxy subsamples: 1) mass limited ($M_* \geq 2 \times 10^{10} M_\odot$; 903 galaxies); 2) mass and SFR limited ($SFR \geq 3 M_\odot \text{ yr}^{-1}$; 308 galaxies, SFRs are defined in §4.1.3); and 3) mass and morphology-limited (Sérsic index $n > 2.5$; 493 galaxies).

4.1.3. Estimating SFR from the UV and IR

We divide the galaxies of each subsample into four even ($\Delta z = 0.2$) redshift slices. Average UV and IR luminosities are estimated for galaxies in each redshift bin and each sample. We use stacking techniques to estimate the average fluxes of individually undetected objects in a subset of galaxies (see Zheng et al. 2006 for details about the $24 \mu\text{m}$ stacking). This is important for obtaining a complete SFR estimate for massive spheroid-dominated galaxies because most such galaxies are intrinsically faint in the UV and mid-IR. The stacked

¹¹ Surface brightness dimming is likely to introduce a redshift-dependent systematic effect. Disk components (typically of relatively lower-surface brightness) will probably be less frequently detected at higher redshifts (see Shi et al. 2009, for a related discussion). A tendency towards a higher fraction of disk contamination in higher-redshift spheroids could result, affecting the inferred redshift evolution of the SFR density in $n > 2.5$ systems.

TABLE 2
AVERAGE SFR AND STELLAR MASS FOR THREE GALAXY SUB-POPULATIONS
OVER $0 < z < 1$.

z	N_{obj}	$\langle SFR \rangle$ ($M_\odot \text{ yr}^{-1}$)	$\langle M_* \rangle$ ($10^{10} M_\odot$)	ρ_{SFR} ($10^{-2} M_\odot \text{ yr}^{-1} \text{ Mpc}^{-3}$)
massive galaxies				
0.04	0.4 ± 0.2
0.3	64	3.1 ± 0.2	5.0 ± 0.5	1.1 ± 0.5
0.5	230	4.3 ± 0.2	4.5 ± 0.6	1.2 ± 0.4
0.7	421	8.3 ± 0.3	5.7 ± 0.5	2.5 ± 0.7
0.9	188	15.1 ± 0.8	5.5 ± 0.7	3.5 ± 1.9
massive spheroid-dominated galaxies				
0.04
0.3	35	0.9 ± 0.1	4.5 ± 0.8	0.22 ± 0.12
0.5	122	1.3 ± 0.1	6.4 ± 0.8	0.22 ± 0.07
0.7	249	4.2 ± 0.2	6.7 ± 0.7	0.65 ± 0.19
0.9	87	9.1 ± 0.8	6.8 ± 1.2	1.01 ± 0.59
massive $SFR \geq 3 M_\odot \text{ yr}^{-1}$ galaxies				
0.04	0.2 ± 0.1
0.3	19	7.1	4.1	0.7 ± 0.4
0.5	89	10.2	4.9	1.1 ± 0.6
0.7 ^a	176	15.2	4.5	$> 1.9 \pm 0.8$
0.9 ^a	81	23.0	4.6	$> 2.3 \pm 1.4$
massive $SFR \geq 10 M_\odot \text{ yr}^{-1}$ galaxies				
0.04	0.04 ± 0.03
0.3	3	14.3	5.9	0.2 ± 0.1
0.5	29	20.2	4.9	0.7 ± 0.2
0.7	99	22.0	4.8	1.6 ± 0.5
0.9	63	27.4	4.0	2.1 ± 1.2

^a Sample is incomplete in this redshift bin. The average SFR is overestimated and the volume-averaged SFR is underestimated.

fluxes and individually detected fluxes are combined to obtain the mean flux for the given subset of galaxies. This procedure was applied to MIPS $24 \mu\text{m}$ and GALEX FUV and NUV. Average FUV, NUV and $24 \mu\text{m}$ luminosities are obtained for each subset of galaxies. Optical photometry in the U, B, V, R and I bands from the COMBO-17 survey is available for all individual sample galaxies, allowing calculation of the average luminosities in these bands.

The total UV luminosity is estimated by integrating the spectral energy distributions over the wavelength range of rest-frame 1500 - 2800 Å from linear interpolation of the FUV, NUV and optical U, B, V, R and I bands. We estimate the total IR luminosity from the observed $24 \mu\text{m}$ luminosities using three sets of luminosity-dependent IR SED templates (Lagache et al. 2004; Dale & Helou 2002; Chary & Elbaz 2001).¹² Although these templates are derived from local star-forming galaxies, they can be used to represent IR SEDs for distant star-forming galaxies (Marcellac et al. 2006; Zheng et al. 2007; Magnelli et al. 2009). We calculate the SFR from the UV and IR luminosities assuming a Kroupa IMF, following Bell et al. (2005). Average SFR values are therefore obtained for each subset of galaxies split by redshift in three samples. We combine bootstrap errors with scatter between templates to compute errors in estimating the SFR. Systematic errors in estimating SFR have not been included explicitly, but are discussed in Bell et al. (2005) and Zheng et al. (2006). We also compute the average stellar mass for each subset of sample galaxies using stellar mass estimates obtained from COMBO-17 optical SEDs by Borch et al. (2006). Table 2 lists the results, including object number, average SFR, average stellar mass and volume-averaged SFR for our samples.

¹² Adoption of the updated IR SED templates based on Spitzer observations (Rieke et al. 2009) gives consistent results within the uncertainties.

We further calculate the SFR for sample galaxies that are individually detected at $24\mu\text{m}$. The IR luminosities of these galaxies typically dominates ($> 80\%$) the bolometric luminosity (UV+IR). The 5σ detection limit of our $24\mu\text{m}$ imaging is $83\mu\text{Jy}$. This limit corresponds to an IR luminosity $\sim 3(10) \times 10^{10} L_{\odot}$ and a SFR roughly $\sim 3(10) M_{\odot} \text{yr}^{-1}$ at $z = 0.6$ (1). Our sample of massive galaxies with $SFR \geq 3 M_{\odot} \text{yr}^{-1}$ is therefore incomplete at $z > 0.6$; a cut of $SFR \geq 10 M_{\odot} \text{yr}^{-1}$ is complete up to $z = 1$. We bear this in mind and discuss its effects on the relevant conclusions.

We could simply use the SFR density determined from the ECDFS alone in what follows, by simply dividing the total amount of SFR in these subsamples by the survey volume. That approach would give very similar results to those that we present later (with the exception of the $0.6 < z < 0.8$ bin, where a somewhat higher SFR density would be determined owing to the overdensity in the ECDFS at $0.6 < z < 0.8$), and our conclusions would be unchanged. Yet, we choose to use a slightly more complex approach that attempts to reduce field-to-field variance by comparing the ECDFS to the rest of the COMBO-17 survey. We adjust the SFR densities for the massive galaxy samples by multiplying by the ratio of the average stellar mass density derived for all of COMBO-17 to the stellar mass density in massive galaxies in the ECDFS: i.e., $SFR_{\text{all}} \sim SFR_{\text{ECDFS}} \times \rho_{*,\text{all}}/\rho_{*,\text{ECDFS}}$. Similarly, we adjust the inferred SFR density in spheroid-dominated galaxies using the stellar mass density in red-sequence galaxies from Borch et al. (2006) as a guide (see McIntosh et al. 2005, for the comparison between mass functions of morphology-selected and color-selected early-type galaxies): $SFR_{n>2.5,\text{all}} \sim SFR_{n>2.5,\text{ECDFS}} \times \rho_{*,\text{red,all}}/\rho_{*,\text{red,ECDFS}}$.

4.1.4. Local comparison sample

We augment the intermediate-redshift sample with a sample of 2177 local galaxies collected from the NASA/IPAC Extragalactic Database (NED) to assess the corresponding volume-averaged SFR at $z \sim 0$ for the three sub-populations. The sample galaxies are selected with a 2MASS K -band magnitude cut $K < 12$ in the volume of $1500 \leq cz \text{ (km s}^{-1}) \leq 3000$ and Galactic latitude $b > 30^{\circ}$. About 61% of the selected galaxies have redshifts from NED. We believe that the redshift identification is not significantly biased and the sample is representative of local galaxies. Details about the sample completeness can be found in Bell et al. (2005). Stellar masses were estimated from the K -band absolute magnitude assuming a K -band stellar mass-to-light ratio of $0.6 M_{\odot}/L_{\odot}$ and a Kroupa IMF (Bell et al. 2003). Of the 2177 sample galaxies, 1089 have IRAS 60 and $100\mu\text{m}$ detections. The IRAS detection limit of $\sim 3 \times 10^{-11} \text{ ergs cm}^{-2} \text{ s}^{-1}$ is applied to the remaining 1088 galaxies. The total IR luminosity derived from IRAS observations is used to estimate the SFR following Bell (2003). The typical error is ~ 0.3 dex for both stellar mass and SFR. We calculated the volume-averaged SFR for the mass limited subsample, and for the mass and SFR limited subsample. The morphological Sérsic index parameter is not available for this local sample, so the volume-averaged SFR at $z = 0$ is missing for the mass and morphology limited subsample. We note that the local comparison sample provides roughly consistent results with the optically-selected sample from the SDSS (Schiminovich et al. 2007), although a small offset exists between the two mainly due to the difference in SFR estimator.

4.1.5. Results

TABLE 3
BEST-FIT PARAMETERS FOR THE INCREASES OF VOLUME-AVERAGED SFR/BHAR OF GALAXY/AGN SUB-POPULATIONS WITH LOOKBACK TIME.

population	A ^a	B ^a	Ref. ^b
all galaxies	0.11 ± 0.01	-2.03 ± 0.03	this work
massive ^c	0.12 ± 0.05	-2.43 ± 0.26	this work
massive & $n > 2.5$	0.18 ± 0.11	-3.40 ± 0.61	this work
massive & $SFR \geq 3$	0.14 ± 0.06	-2.63 ± 0.28	this work
massive & $SFR \geq 10$	0.25 ± 0.06	-3.46 ± 0.31	this work
AGN ($\log L_{\text{bol}} > 43$)	0.17	-2.24	H07,M04
AGN ($\log L_{\text{bol}} > 44.9$)	0.21	-2.73	H07,M04
AGN ($\log L_{\text{bol}} > 45.5$)	0.23	-3.03	H07,M04

^a Best fit parameters for $\log \rho_{\text{SFR}} = A t_{\text{LB}} + B$ (galaxies) or $\log \rho_{\text{BH}} + 3.11 = A t_{\text{LB}} + B$ (AGN) over the redshift range $0 < z < 1$, where t_{LB} is the lookback time in units of Gyr. The constant 3.11 is the scaling factor 1300 in logarithm.

^b References — B07: Bell et al. (2007); LF05: Le Floch et al. (2005); H07: Hopkins et al. (2007b); M04: Marconi et al. (2004);

^c Refer to $M_{*} \geq 2 \times 10^{10} M_{\odot}$.

Figure 4 shows the volume-averaged SFR as a function of the lookback time for three galaxy subsamples. For comparison, we also show the volume-averaged SFR density for all galaxies (§2.1; thick gray line). All three galaxy subsamples have a higher average SFR at larger redshift, consistent with the overall galaxy population. A straight line is fit to the data points, accounting for the error bars on both axes.¹³ The line is described by $\log \rho_{\text{SFR}} = A t_{\text{LB}} - B$, where ρ_{SFR} is the volume-averaged SFR and t_{LB} is the lookback time in units of Gyr. The best-fit parameters given by the error-weighted least-squares fit are listed in table 3.

Integration of the volume-averaged SFR over $0 < z < 1$ shows that massive galaxies contribute 45% to the overall volume-averaged SFR. Most of this SFR ($> 85\%$) is contained in the mass-limited subsample defined to have $SFR > 3 M_{\odot} \text{yr}^{-1}$; this reflects that the typical SFR of a massive star-forming galaxy is $\gtrsim 3 M_{\odot} \text{yr}^{-1}$ (Noeske et al. 2007). A subsample limited at $> 10 M_{\odot} \text{yr}^{-1}$ contains 43% of the SFR in massive galaxies.

Star formation in the host galaxies of X-ray-detected AGN is not counted. The difficulty in estimating star formation in these galaxies is how to separate the IR emission powered by star formation from that by AGN. We note that the removal of X-ray detected sources in our sample selection does not influence our results. Indeed, the $24\mu\text{m}$ fluxes from the X-ray detected sources are negligible compared with the total $24\mu\text{m}$ fluxes from those X-ray undetected ones ($< 15\%$; see also Brand et al. 2006). The average SFR is dominated by galaxies without significant AGN, indicating that SF and BH accretion take place in different phases or over different time intervals.

4.1.6. Hosts of star formation: spheroids or disks?

About one quarter of the SF in massive galaxies is contained in ‘spheroid-dominated’ galaxies with $n > 2.5$; given that 45% of the total SFR density at $z \lesssim 1$ is contained in the massive galaxy sample, this result is consistent with earlier results that found that $< 10\%$ of all SF is in lenticular or elliptical galaxies (Bell et al. 2005).

Our SFR estimates measure the SF in the whole galaxy. The IR data we use do not have sufficient spatial resolution

¹³ The vertical error shows the random uncertainties in SFR density. The horizontal “errorbar” indicates the redshift range and the data points are uniformly weighted in redshift space.

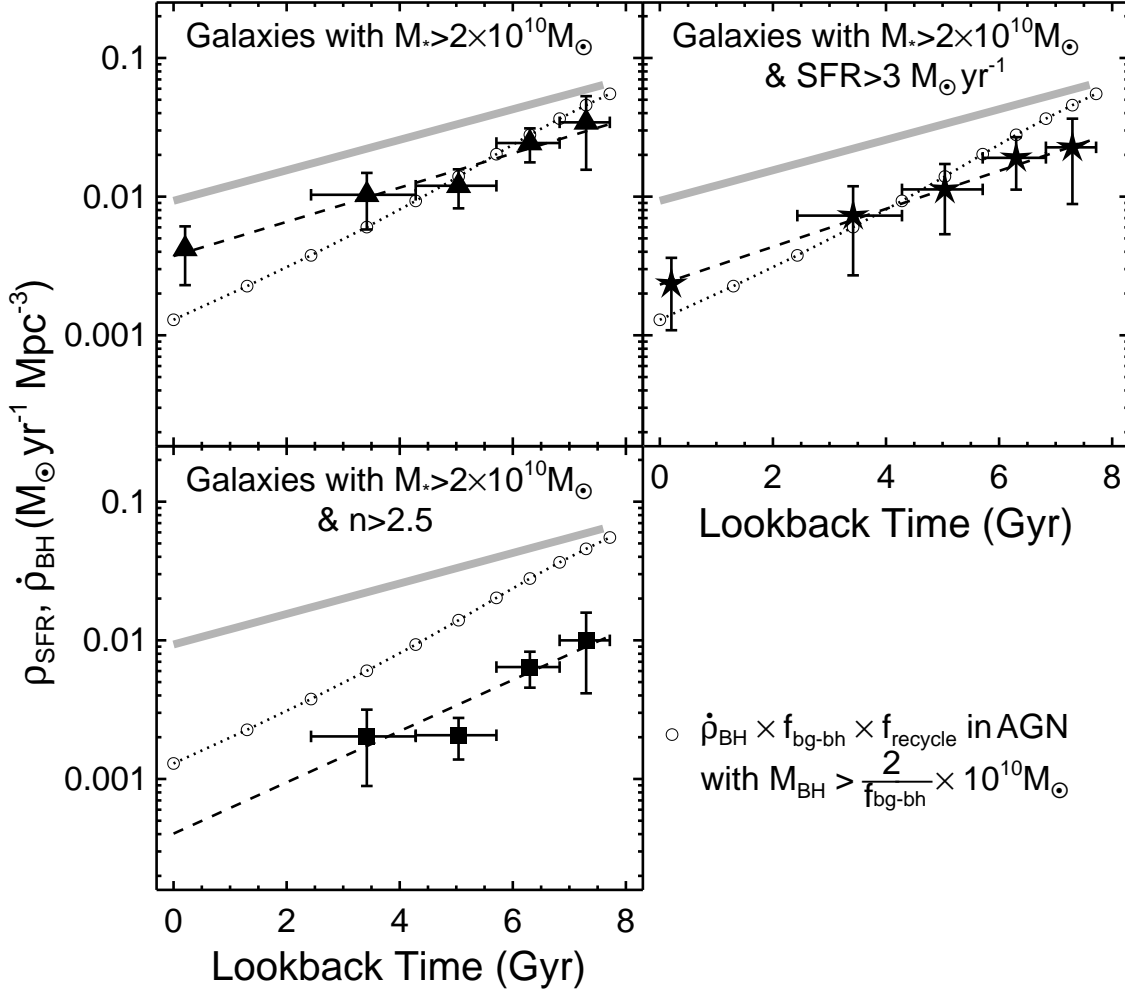


FIG. 4.— The volume-averaged SFR as a function of lookback time for massive ($M_* \geq 2 \times 10^{10} M_\odot$) galaxies (top-left), massive high-SFR ($SFR \geq 3 M_\odot \text{ yr}^{-1}$) galaxies (top-right) and massive spheroid-dominated (Sérsic index $n > 2.5$) galaxies (bottom-left). Horizontal errorbars represent the redshift range and vertical errorbars represent 1σ errors derived from bootstrapping. The dashed lines show least-squares fits to data points (taking into account the errorbars on both axes). The gray thick line in each panel is the least-squares fit to all data points at $z < 1$ listed in Figure 1, giving best estimates of the global volume-averaged SFR. The dotted lines are the same in all three panels, showing the volume-averaged BHAR attributed to luminous AGN ($L_{\text{bol}} \geq 10^{44.9} \text{ erg s}^{-1}$) converted from the best-fit LDDE model of the bolometric LFs given in HRH07 with a radiation efficiency $\epsilon = 0.1$, scaled by a factor of $f_{\text{bg-bh}} \times f_{\text{recycle}}$. Here $f_{\text{bg-bh}}$ is the local M_{BH}/M_* ratio of 650 given by the local BH-bulge mass relation (Häring & Rix 2004), and f_{recycle} is the recycling factor. We adopt $f_{\text{recycle}} = 2$. Assuming an average Eddington ratio $\log(L_{\text{bol}}/L_{\text{Edd}}) = -0.60 \pm 0.3$ for luminous AGN (Kollmeier et al. 2006), the bolometric luminosity $L_{\text{bol}} \geq 10^{44.9} \text{ erg s}^{-1}$ corresponds to BH mass $M_{\text{BH}} \geq 2.6 \times 10^7 M_\odot$ and accordingly spheroid mass $2 \times 10^{10} M_\odot$.

to distinguish between SF in spheroidal and disk components within a galaxy. Accordingly, we adopted a simplistic approach of assigning all SF in concentrated $n > 2.5$ spheroid-dominated galaxies to spheroids (an overestimate), and assigning all SF in $n < 2.5$ disk-dominated systems to disks (some of that SF may be in spheroids in these disk-dominated galaxies; this would drive one towards underestimating the SFR in disks). While mid-IR imaging data from JWST will help to address this problem in the long-term, our present approach is essentially all that the current data support, and provides a reasonable guide to the possible contribution of spheroids to the volume-averaged SFR density. Bearing in mind the caveats, we conclude nonetheless that the bulk of the overall SF is associated with disks, rather than spheroids; we estimate that $< 30\%$ of SF in massive galaxies can be associated with $n > 2.5$ spheroid-dominated galaxies at any epoch in the last 8 Gyr.

4.2. BH accretion in Luminous AGN

It would be ideal to measure the BH accretion rate for our sample of galaxies in the ECDFS. Unfortunately, episodes of intense accretion by supermassive black holes are rare, and the number of AGN in the ECDFS is too low to allow an analysis as detailed as our above discussion of the SFR density. Accordingly, we here adopt an intermediate approach based on luminosity-selected samples (derived from larger-area surveys) that gives a good estimate of the BHAR density in the massive galaxy population.

It is generally assumed that BH accretion obeys the Eddington limit. A luminous AGN is normally caused by intense accretion onto a massive BH, while a faint AGN can be due to either a massive BH with low accretion rate or a less massive BH with higher accretion rate. Kollmeier et al. (2006) found that luminous AGN have an average Eddington ratio $L_{\text{bol}}/L_{\text{edd}} \approx 0.25$ with a scatter of 0.3 dex over a wide redshift

range. This implies a strong correlation between AGN luminosity and BH mass.

We want to estimate the BHAR in massive BHs in galaxy populations of mass $M_* \geq 2 \times 10^{10} M_\odot$, and compare it to the SFR in the same galaxies. According to the local BH-bulge mass relation given by Häring & Rix (2004), spheroids with mass $M_* \geq 2 \times 10^{10} M_\odot$ host SMBHs with mass $M_{\text{BH}} \geq 2.6 \times 10^7 M_\odot$. Combined with the local mass function from Bell et al. (2003), we assume a mean spheroid-BH mass ratio $M_*/M_{\text{BH}} = 650$ for local massive spheroid-dominated galaxies. Assuming Eddington ratio $L_{\text{bol}}/L_{\text{edd}} = 0.25$ and radiation efficiency $\epsilon = 0.1$, we infer that massive BHs of $M_{\text{BH}} \geq 2.6 \times 10^7 M_\odot$ power luminous AGN of $\log L_{\text{bol}} \geq 44.9$ with $\text{BHAR} \geq 0.13 M_\odot \text{ yr}^{-1}$. We have seen that such intense BH accretion events statistically match starburst events with $\text{SFR} \geq 3 M_\odot \text{ yr}^{-1}$, according to the universal agreement between BH accretion events and SF events (a factor of 20 in intensity; see §3).

If the local BH-bulge mass relation holds at all cosmic epochs, then the mass growth of SMBHs and that of spheroids should follow the same relation as $\frac{\langle \dot{M}_* \rangle}{\langle \dot{M}_{\text{BH}} \rangle} = 650$. We use the best-fit LDDE model of bolometric LFs from HRH07 to calculate the volume-averaged BHAR contained in luminous AGN of $\log L_{\text{bol}} \geq 44.9$ over $0 < z < 1$. The results are scaled up by a factor of 1300 and shown with the dotted lines in Figure 4 (same in all four panels). The scaling factor 1300 accounts for the mean local spheroid-BH mass ratio 650 and the recycling factor of two. Note that some studies (e.g. Treu et al. 2007) have claimed to find evidence that the BH-spheroid mass ratio was larger in the past (although see Lauer et al. (2007b)). If this is the case, it would obviously invalidate the “strong” co-evolution picture. It would impact our calculation by changing the slope of the BHAR function when cut by the “matching” BH mass, because a given bulge mass would correspond to a larger BH mass and therefore to a higher AGN luminosity at high redshift. We discuss the implications of such an effect in Section 5.

The open circles mark redshifts from $z = 0$ to $z = 1$ with a step size $\Delta z = 0.1$. We fit a straight line to these points and present the best-fit parameters given by the least-squares fit in Table 3. In addition, we also fit the overall BHAR (in AGN of $\log L_{\text{bol}} > 43$) and tabulate the corresponding best-fit parameters in Table 3. We estimate that luminous ($\log L_{\text{bol}} \geq 44.9$) and very luminous ($\log L_{\text{bol}} \geq 45.5$) AGN are responsible for $\sim 70\%$ and $\sim 45\%$ of the overall BH accretion over $0 < z < 1$, respectively. We caution that the correspondence between AGN luminosity and BH mass depends on the Eddington ratio. The uncertainty of 0.3 dex in the Eddington ratio (Kollmeier et al. 2006) causes a negligible error in the sum of the intense BH accretion. The scatter in the local BH-bulge relation (~ 0.3 dex) introduces a comparable error. It is worthwhile to note that the Eddington ratio may be luminosity dependent: it is possibly close to unity for luminous quasars and increasingly sub-Eddington for low-luminosity AGN (Babić et al. 2007; Bundy et al. 2008). If so, our calculations will underestimate the accretion for massive BHs. However, as long as the *average* accretion rate for the objects we include in our calculation is similar to that of the Kollmeier et al. sample, our results should be reasonably accurate. In any case, the overall BH accretion is almost certainly dominated by luminous AGN associated with massive BHs. We emphasize that our conclusions essentially rely on the relative density, i.e., the BHAR density of luminous AGN

to the total, and are marginally affected by how the numbers are calibrated.

4.3. Host galaxy connections

We showed in §4.1.5 that $\sim 45\%$ of SF happens in massive galaxies ($M_* \geq 2 \times 10^{10} M_\odot$). We estimated in §4.2 the total amount of BH accretion in massive galaxies using an accretion rate-limited sample, in conjunction with an assumption about the distribution of Eddington ratios, to conclude that $\sim 70\%$ of BH accretion should be contained in the massive galaxy population. The uncertainties inherent in our analysis in §4.2 are considerable, but it appears that the bulk of BH accretion tends to occur in massive systems, whereas much of the SF happens in lower mass systems.

Furthermore, we showed in §4.1.6 that $< 30\%$ of the star formation in massive galaxies ($M_* \geq 2 \times 10^{10} M_\odot$) happens in spheroid-dominated systems: star formation, to first order, happens in disks. Although a substantial fraction of AGN by number reside in late- and intermediate-type galaxies (Pierce et al. 2007; Gabor et al. 2009), the luminous ones tend to reside in massive, early-type galaxies. Therefore, it is clear that the bulk of the black hole accretion happens in spheroid-dominated galaxies: it appears that BH accretion is happening in different objects or at a different phase in the life-cycle of galaxies than the bulk of the star formation.

We illustrate this point with an example from the ECDFS (this exercise simply reinforces the conclusions of, e.g., Grogin et al. 2005; Nandra et al. 2007; Pierce et al. 2007; Georgakakis et al. 2008; Alonso-Herrero et al. 2008; Gabor et al. 2009). We select massive galaxies with $M_* > 2.5 \times 10^{10} M_\odot$ in the redshift range $0.4 < z < 0.8$ in the ECDFS to create a parent sample. From the sample, we select those detected in the 250 ks *Chandra* X-ray observation (Lehmer et al. 2005) to make a subsample of galaxies having luminous AGN with soft X-ray luminosity $> 10^{42} \text{ erg s}^{-1}$. The IR-detected galaxies, i.e. those detected at $24 \mu\text{m}$, are selected to comprise a subsample of star-forming galaxies (see §4.1.3 for the details of the MIPS $24 \mu\text{m}$ observation and Donley et al. 2008, for further discussion). This subsample is also limited to have soft X-ray luminosities $< 10^{42} \text{ erg s}^{-1}$ to avoid AGN contamination to the IR. Sérsic indices are derived for all sample galaxies from their GEMS/ACS images (Häußler et al. 2007). The X-ray-detected AGN are generally obscured in the optical and contribute marginal contamination ($< \sim 10\%$ of central flux) to their host galaxies. Therefore the Sérsic index is derived from the GEMS/ACS imaging of the host galaxies is insensitive to the central AGN. Figure 5 shows the histograms of Sérsic index n for all galaxies, subsamples of IR-detected galaxies and X-ray-detected galaxies. One can see that two thirds of X-ray-detected galaxies have $n > 3$, while two thirds of IR-detected galaxies have $n < 3$, suggesting that the X-ray-detected AGN host galaxies are more concentrated than the IR-detected star-forming galaxies. A Kolmogorov-Smirnov (K-S) test indicates that the probability for both distributions to be drawn from the same distribution is less than 10^{-9} , implying that the IR-detected galaxies and X-ray-detected galaxies are different populations. Put simply, star formation and SMBH accretion take place in dramatically different systems: the majority of the global star formation happens in late-type galaxies (i.e. disks), while the dominant phases of BH accretion occur in intermediate- and early-type galaxies.

5. SUMMARY AND DISCUSSION

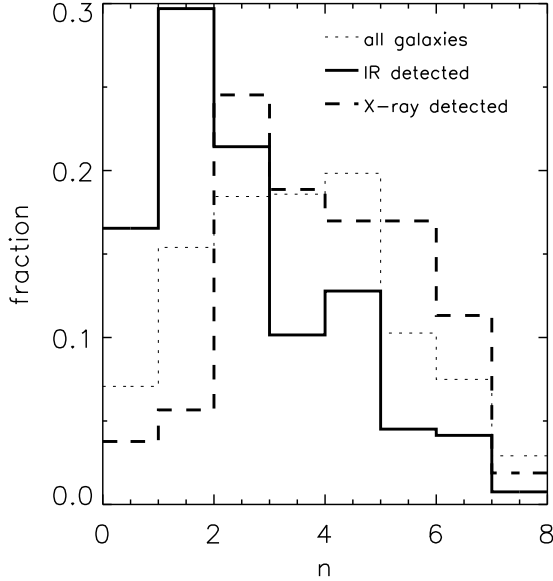


FIG. 5.— Histograms of Sérsic index n for IR-detected galaxies (the thick solid line) and X-ray-detected galaxies (the thick-dashed line) for galaxies with $M_* > 2 \times 10^{10} M_\odot$ and $0.4 < z < 0.8$. Here the IR-detected galaxies refer to star-forming galaxies detected at $24 \mu\text{m}$ and with soft X-ray luminosity $< 10^{42} \text{ erg s}^{-1}$. The X-ray-detected galaxies are those detected in the *Chandra* soft band with X-ray luminosity $> 10^{42} \text{ erg s}^{-1}$, suggestive of AGN activity. The X-ray-detected AGN host galaxies are more concentrated than the IR-detected star-forming galaxies.

We have shown that the global SF history is proportional to the global BH accretion up to (at least) $z \sim 1$, and the proportionality factor (2000) is that expected if the BHAR is a fixed fraction of the star formation that ends up in galactic bulges. This parallel between the cosmic SF history and the cosmic BH accretion history is an important constraint on the co-evolution between SMBHs and galaxies. It suggests that *overall* accretion-driven BH growth and *overall* SF-driven galaxy growth trace each other, and that the globally averaged BH mass to stellar mass ratio remains constant. Furthermore, we find that the SFR and BHAR *multiplicity functions* are also scaled versions of one another at $z < 1$, suggesting that the intensity of star formation and BH accretion are at least statistically linked.

We then refined our analysis to test the hypothesis that star formation and BH accretion do not just trace each other in a statistical fashion, but that *the SFR and BHAR are related by a fixed factor* $f_{\text{co}} \equiv f_{\text{recycle}} f_{\text{bg-BH}} \approx 1300$ in every bulge/BH-building event. We focused our analysis on massive galaxies with $M_* > 2 \times 10^{10} M_\odot$, for which our observational sample is complete to $z \sim 1$. Assuming that the local relationship between BH mass and bulge mass remains constant, spheroids with $M_* > 2 \times 10^{10} M_\odot$ should host BH with mass $M_{\text{BH}} \geq 2.6 \times 10^7 M_\odot$. Assuming an average Eddington ratio $L_{\text{bol}}/L_{\text{Edd}} = 0.25$ (Kollmeier et al. 2006), and $\epsilon = 0.1$, these BH, when active, power AGN with $\text{BHAR} \geq 0.13 M_\odot \text{ yr}^{-1}$ or bolometric luminosity $\log L_{\text{bol}} \geq 44.9$. We computed the BHAR contributed by AGN with bolometric luminosities above this limit, and compared it with the SFR contributed by galaxies with $M_* > 2 \times 10^{10} M_\odot$. We found that the SFR and BHAR again trace each other but are offset by approximately the factor of $f_{\text{co}} \approx 1300$ expected for massive spheroid-dominated galaxies. This result is nearly unchanged

if we compute the SFR from galaxies limited in both stellar mass and SFR ($\text{SFR} \geq 3 M_\odot \text{ yr}^{-1}$), as these “high-intensity” SF events dominate the SFR budget in massive galaxies. The massive galaxies are simply dominating the total SFR, and the big accretion systems are dominating the accretion history (although with a little more evolution). Just as before when we compared the overall SFRD with the overall BHAR we got a match, we should get a match for the top two panels.

Further examination of the nature of the galaxies hosting star formation and BH activity showed that only about 30 % of the SF “budget” needed to match the BHAR is observed in massive *spheroid dominated* galaxies. Furthermore, the distribution of Sérsic indices for star forming galaxies and that for AGN detected in the soft X-ray indicate that these two classes of activity tend not to reside in the same types of host galaxies. The bulk of star formation occurs in *isolated disks* while the majority of luminous AGN hosts are intermediate- and early-type galaxies (see also Grogin et al. 2005; Nandra et al. 2007; Georgakakis et al. 2008; Alonso-Herrero et al. 2008; Watson, et al. 2009; Gabor et al. 2009). These results clearly rule out the simplest picture of object-by-object co-evolution, in which BH and bulges grow proportionally and simultaneously. This is also supported by the detection of a small fraction of luminous X-ray detected AGN in spirals, indicating that BH accretion may happen in non-bulge-building events (e.g., Georgakakis et al. 2009).

There are both observational claims and theoretical expectations that the relationship between BH mass and spheroid mass might have been larger in the past. While this evolution would impact our calculation by shifting the mass of the BH (and therefore the cutoff luminosity for AGN) to include in our “matched” BHAR, this would only cause a minor change in the slope of the BHAR and cannot remove the mismatch between SF and BHA in spheroid dominated galaxies. Therefore, this would not change any of our conclusions.

There are two possible ways to reconcile this apparent paradox. One possibility (which shall now call Merger Scenario 1) is that bulges and BH grow in proportion to one another, and in the same *events*, but with an offset in time. For example, in simulations of galaxy-galaxy mergers including BH growth, the luminous AGN phase is delayed by about a dynamical time (a few hundred Myr) relative to the peak of the starburst activity (Di Matteo et al. 2005; Hopkins et al. 2005, 2006). In this picture, we would expect that most AGN hosts would resemble late-stage mergers, i.e. objects with spheroidal morphology but young stellar populations, in plausible agreement with our observational results. Moreover, in this picture, we would expect that a small fraction of AGN to be detected in early stage mergers, and the star formation associated with this BH growth should be observed in early-stage mergers, i.e. close pairs or highly morphologically disturbed objects.

However, other studies have found that only a small fraction of the global star formation at $z < 1$ is occurring in galaxy mergers (Bell et al. 2005; Wolf et al. 2005; Jogee et al. 2009; Robaina et al. 2009): the strongest limit is set by Robaina et al., who find that $< 10\%$ of the star formation in massive galaxies ($m_* > 10^{10} M_\odot$) is directly triggered by *all identifiable phases* (from close pairs to morphologically disturbed remnants) of major galaxy merging. This is strong evidence against the Merger Scenario 1. Therefore, while a small fraction of the star formation associated with the BH growth that we witness at $z \lesssim 1$ may be occurring in the same merger events that feed the BH, it seems that this does not represent the majority of the SF activity needed to “match” the observed

BH accretion.

The second possibility (Merger Scenario 2) is that most star formation takes place in isolated disks. When these disks merge, the pre-existing stars are scrambled into a dynamically hot spheroidal remnant¹⁴. The presence of even a modest amount of gas leads to the formation of a remnant with higher phase-space density and hence a deeper gravitational potential well (Dekel & Cox 2006; Robertson et al. 2006b; Cox et al. 2006). If the depth of the potential well in the central parts of the galaxy determines how large the BH can grow, as in the picture of self-regulated BH growth outlined by Hopkins et al. (2007a), then the post-merger BH will end up on the BH mass-bulge mass relation, *despite the fact that the SFR and BHAR during the merger event may not necessarily obey the universal proportionality factor*.

One can easily see that in this scenario, in many cases the BH accretion and the star formation will not trace each other during the merger event. For example, in a major merger of two pure disk progenitors, the scaled BHAR will be larger than the SFR associated with bulge growth. Most of the bulge mass will be contributed by the pre-existing stars in the progenitor disks, and the BH will grow to “catch up” with the bulge. In the opposite extreme, in a merger of two galaxies with pre-existing massive BH, there may be very little BH accretion because the AGN will almost immediately “shut itself off”. In this case, the SF in the merger might be larger than the scaled BH accretion (if the progenitors contain enough gas).

Because what we see is more BH accretion than we would expect based on the amount of star formation in spheroids, we conclude that most of the mass in these spheroids was contributed by the pre-existing stars in the progenitors rather than by new stars formed in the merger-associated bursts. Indeed, we have independent lines of evidence that this must be the case. We know that the colors of elliptical galaxies and bulges at $z \lesssim 1$ are characteristic of fairly old stellar populations (Gallazzi et al. 2006; Renzini 2006, and references therein), and similarly, fossil evidence from line strengths in nearby ellipticals also precludes the very recent formation of a large fraction of the stellar mass (Trager et al. 2000; Thomas et al. 2005). In addition, this picture is consistent with the relatively small fraction of star formation associated with ongoing mergers at $z < 1$: in cosmological models that incorporate a scenario like Merger Scenario 2 (e.g. Somerville et al. 2008), the predicted fraction of star formation triggered by major mergers at $z < 1$ is about 7%, in excellent agreement with the observational estimates (see Robaina et al. 2009 for details of the comparison).

A slightly modified version of Merger Scenario 2 can also be accommodated in a Universe in which the BH-spheroid mass ratio has decreased with time. This is in fact expected in the theoretical picture that has emerged from the analysis of hydrodynamic simulations of galaxy mergers with self-regulated BH growth (e.g. Robertson et al. 2006a; Hopkins et al. 2007a). These studies find that the

final BH-spheroid mass ratio depends on the gas fraction of the progenitors. This is because gas-rich progenitors can dissipate energy during the merger, and all else equal, form more compact remnants than gas-poor mergers (Dekel & Cox 2006; Robertson et al. 2006b; Cox et al. 2006; Covington et al. 2008). In this deep potential well, the BH can grow to a larger mass (relative to the spheroid) before the pressure-driven outflow halts further accretion. If gas fractions in merging galaxies were higher at high redshift, as is generally expected, this would then lead to the prediction that BH were more massive relative to their spheroids at high redshift. A significant fraction of mergers at $z < 1$ are expected to involve at least one galaxy that already contains a massive BH. If the pre-existing BH is already larger than the “critical mass” set by the new remnant, further BH growth will be stifled. Theoretical models predict that this expected evolution is relatively mild: less than a factor of two since $z \sim 1$ (Hopkins et al. 2007a).

Borch et al. (2006) have shown that the stellar mass in red (predominantly spheroidal) galaxies has increased by a factor of 2–3 since $z \sim 1$, while the stellar mass in blue (disk-dominated) galaxies has remained about the same over this time period. At the same time, we know that the bulk of new star formation is occurring in blue (disk-dominated) galaxies, implying that mass in blue (disk) galaxies must be transformed into red (spheroidal) galaxies at approximately the same rate that new stars are forming (Bell et al. 2007). Given that most of the red galaxies are spheroid-dominated, which is well established at least at $z < 1$ (Bell et al. 2004a), the mass on the red sequence cannot grow simply via the quenching of star formation in disks — a strong dynamical process like merging is required.

Taken together, this evidence strongly favors a picture in which, at least at $z < 1$, the bulk of the growth of mass in spheroids is due to merging of pre-existing, already old disk stars, and BHs preferentially grow to “catch up” to their newly assembled bulges following a merger event. In this case, the parallel evolution of the global SFR and BHAR may simply reflect the apparent coincidence that, at $z < 1$, the rate of formation of new stars is approximately equal to the rate that stellar mass is transferred from disks into bulges via mergers.

We thank the referee for valuable comments that improved this manuscript. X. Z. Z. is supported by NSFC under grant 10773030, 10833006 and by the National Basic Research Program of China (973 program; 2007CB815404). E. F. B. and K. J. thank the Deutsche Forschungsgemeinschaft for their support through the Emmy Noether Program. This research has made use of the NASA/IPAC Extragalactic Database (NED) which is operated by the Jet Propulsion Laboratory, California Institute of Technology, under contract with the National Aeronautics and Space Administration.

¹⁴ In what follows, much of what we argue for merger scenario 2 would also apply if the main route for forming low-mass spheroids were secular evolution. The key point for this paper is that the bulk of the stars that end

up in the spheroid are formed long before the epoch of actual bulge creation, which applies equally in Merger Scenario 2 and secular evolution.

REFERENCES

- Alexander, D. M., Smail, I., Bauer, F. E., Chapman, S. C., Blain, A. W., Brandt, W. N., & Ivison, R. J. 2005, *Nature*, 434, 738
 Alonso-Herrero, A., et al. 2008, *ApJ*, 677, 127
 Babic, A., Miller, L., Jarvis, M. J., Turner, T. J., Alexander, D. M., & Croom, S. M. 2007, *A&A*, 474, 755
 Barger, A. J., Cowie, L. L., Mushotzky, R. F., Yang, Y., Wang, W.-H., Steffen, A. T., & Capak, P. 2005, *AJ*, 129, 578
 Barth, A. J., Greene, J. E., & Ho, L. C. 2005, *ApJ*, 619, L151
 Baskin, A., & Laor, A. 2005, *MNRAS*, 356, 1029
 Bell, E. F. 2003, *ApJ*, 586, 794

- Bell, E. F., McIntosh, D., Katz, N., & Weinberg, M. D. 2003, *ApJS*, 149, 289
- Bell, E. F. et al. 2004, *ApJ*, 600, 11
- Bell, E. F., et al. 2004, *ApJ*, 608, 752
- Bell, E. F., et al. 2005, *ApJ*, 625, 23
- Bell, E. F., Zheng, X. Z., Papovich, C., Borch, A., Wolf, C., & Meisenheimer, K. 2007, *ApJ*, 663, 834
- Binney, J., & Tabor, G. 1995, *MNRAS*, 276, 663
- Borch, A., et al. 2006, *A&A*, 453, 869
- Borys, C., Smail, I., Chapman, S. C., Blain, A. W., Alexander, D. M., & Ivison, R. J. 2005, *ApJ*, 635, 853
- Bower, R. G., Benson, A. J., Malbon, R., Helly, J. C., Frenk, C. S., Baugh, C. M., Cole, S., & Lacey, C. G. 2006, *MNRAS*, 370, 645
- Boyle, B. J., & Terlevich, R. J. 1998, *MNRAS*, 293, L49
- Brand, K., et al. 2006, *ApJ*, 644, 143
- Brown, M. J. I., et al. 2006, *ApJ*, 638, 88
- Bundy, K., et al. 2008, *ApJ*, 681, 931
- Cattaneo, A., Blaizot, J., Devriendt, J., and Guiderdoni, B. 2005, *MNRAS*, 364, 407
- Chartas, G., Brandt, W. N. & Gallagher, S. C. 2003, *ApJ*, 595, 85
- Chary, R., & Elbaz, D. 2001, *ApJ*, 556, 562
- Covington, M., Dekel, A., Cox, T. J., Jonsson, P., Primack, J. R. 2008, *MNRAS*, 384, 94
- Crenshaw, D. M., Kraemer, S. B., & George, I. M. 2003, *ARA&A*, 41, 117
- Croom, S. M., Smith, R. J., Boyle, B. J., Shanks, T., Miller, L., Outram, P. J., & Loaring, N. S. 2004, *MNRAS*, 349, 1397
- Croton, D. J. 2006, *MNRAS*, 369, 1808
- Croton, D. J., et al. 2006, *MNRAS*, 365, 11
- Cooper, M. C., et al. 2008, *MNRAS*, 383, 1058
- Cox, T. J., Dutta, S. N., Di Matteo, T., Hernquist, L., Hopkins, P. F., Robertson, B., & Springel, V. 2006, *ApJ*, 650, 791
- Dale, D. A., & Helou, G. 2002, *ApJ*, 576, 159
- Dekel, A. & Cox, T. J. 2006, *MNRAS*, 370, 1445
- Dickinson, M., Papovich, C., Ferguson, H. C., & Budavári, T. 2003, *ApJ*, 587, 25
- Di Matteo, T., Springel, V., Hernquist, L. 2005, *Nature*, 433, 604
- Donley, J. L., Rieke, G. H., Rigby, J. R., Pérez-González, P. G. 2005, *ApJ*, 634, 169
- Donley, J. L., Rieke, G. H., Pérez-González, P. G., Barro, G. 2008, *ApJ*, 687, 111
- Drory, N., Salvato, M., Gabasch, A., Bender, R., Hopp, U., Feulner, G., & Pannella, M. 2005, *ApJ*, 619, L131
- Dunne, L., et al. 2008, *MNRAS*, 394, 3
- Fabian, A. C. Sanders, J. S., Allen, S. W., Crawford, C. S., Iwasawa, K., Johnstone, R. M., Schmidt, R. W., & Taylor, G. B. 2003, *MNRAS*, 344, L43
- Fardal, M., Katz, N., Weinberg, D. H., & Davé, R. 2007, *MNRAS*, 379, 985
- Ferrarese, L., & Merritt, D. 2000, *ApJ*, 539, L9
- Fontana, A., et al. 2003, *ApJ*, 594, L9
- Fontanot, F., Monaco, P., Cristiani, S., & Tozzi, P. 2006, *MNRAS*, 373, 1173
- Fontanot, F., Cristiani, S., Monaco, P., Nonino, M., Vanzella, E., Brandt, W. N., Grazian, A., & Mao, J. 2007, *A&A*, 461, 39
- Franceschini, A., Hasinger, G., Miyaji, T., & Malquori, D. 1999, *MNRAS*, 310, L5
- Gabor, J. M., et al. 2009, *ApJ*, 691, 705
- Gallazzi, A., Charlot, S., Brinchmann, J., & White, S. D. M. 2006, *MNRAS*, 370, 1106
- Gebhardt, K., et al. 2000, *ApJ*, 539, L13
- Georgakakis, A., et al. 2008, *MNRAS*, 385, 2049
- Georgakakis, A., et al. 2009, *MNRAS*, 397, 623
- Granato, G. L., De Zotti, G., Silva, L., Bressan, A., & Danese, L. 2004, *ApJ*, 600, 580
- Greene, J. E., & Ho, L. C. 2006, *ApJ*, 641, L21
- Grogin, N. A., et al. 2005, *ApJ*, 627, L97
- Haiman, Z., Ciotti, L., & Ostriker, J. P. 2004, *ApJ*, 606, 763
- Häring, N., & Rix, H.-W. 2004, *ApJ*, 604, L89
- Hasinger, G., Miyaji, T., & Schmidt, M. 2005, *A&A*, 441, 417
- Häußler, B., et al. 2007, *ApJS*, 172, 615
- Ho, L. C. 2007, *ApJ*, 668, 94
- Hopkins, A. M. & Beacom, J. F. 2006, *ApJ*, 651, 142
- Hopkins, P. F., Hernquist, L., Martini, P., Cox, T. J., Robertson, B., Di Matteo, T., & Springel, V. 2005, *ApJ*, 625, L71
- Hopkins, P. F., Hernquist, L., Cox, T. J., Di Matteo, T., Robertson, B., & Springel, V. 2006, *ApJS*, 163, 1
- Hopkins, P. F., Hernquist, L., Cox, T. J., Robertson, B., & Krause, E. 2007a, *ApJ*, 669, 45
- Hopkins, P. F., Richards, G. T., Hernquist, L. 2007b, *ApJ*, 654, 731
- Hopkins, P. F., Hernquist, L., Cox, T. J., & Keres, D. 2008a, *ApJS*, 175, 356
- Hopkins, P. F., Cox, T. J., Keres, D., & Hernquist, L. 2008b, *ApJS*, 175, 390
- Jogee, S., et al. 2009, *ApJ*, 697, 1971
- Kaspi, S., Maoz, D., Netzer, H., Peterson, B. M., Vestergaard, M., & Jannuzi, B. T. 2005, *ApJ*, 629, 61
- Kauffmann, G., & Haehnelt, M. 2000, *MNRAS*, 311, 576
- Kollmeier, J. A., et al. 2006, *ApJ*, 648, 128
- Kormendy, J. 2001, in *ASP Conf. Ser. 230, Galaxy Disks and Disk Galaxies*, ed. J. G. Funes & E. M. Corsini (San Francisco: ASP), 247
- Kroupa, P. 2001, *MNRAS*, 322, 231
- La Franka, F., et al. 2005, *ApJ*, 635, 864
- Lagache, G., et al. 2004, *ApJS*, 154, 112
- Lauer, T. R., et al. 2007, *ApJ*, 662, 808
- Lauer, T. R., Tremaine, S., Richstone, D., Faber, S. M., 2007, *ApJ*, 670, 249
- Le Flo'ch, E., et al. 2005, *ApJ*, 632, 169
- Lehmer, B. D., et al. 2005, *ApJS*, 161, 21
- Magnelli, B., Elbaz, D., Chary, R. R., Dickinson, M., Le Borgne, D., Frayer, D. T., & Willmer, C. N. A. 2009, *A&A*, 496, 57
- Magorrian, J., et al. 1998, *AJ*, 115, 2285
- Marcillac, D., Elbaz, D., Chary, R. R., Dickinson, M., Galliano, F., & Morrison, G. 2006, *A&A*, 451, 57
- Marconi, A., & Hunt, L. K., 2003, *ApJ*, 589, L21
- Marconi, A., Risaliti, G., Gilli, R., Hunt, L. K., Maiolino, R., & Salvati, M. 2004, *MNRAS*, 351, 169
- Martin, D. C., et al. 2005, *ApJ*, 619, L1
- McIntosh, D. H., et al. 2005, *ApJ*, 632, 191
- McNamara B. R., et al. 2000, *ApJ*, 534, L135
- McNamara B. R., Nulsen, P. E. J., Wise, M. W., Rafferty, D. A., Carilli, C., Sarazin, C. L., & Blanton, E. L. 2005, *Nature*, 433, 45
- Merloni, A., Rudnick, G., & Di Matteo, T. 2004, *MNRAS*, 354, L37
- Miyaji, T., Hasinger, G., & Schmidt, M. 2000, *A&A*, 353, 25
- Monaco, P., Fontanot, F., & Taffoni, G. 2007, *MNRAS*, 375, 1189
- Morrissey, P., et al. 2005, *ApJ*, 619, L7
- Murray, N., Quataert, E., & Thompson, T. A. 2005, *ApJ*, 618, 569
- Nandra, K., et al. 2007, *ApJ*, 660, L11
- Noeske, K., et al. 2007, *ApJ*, 660, L43
- Pannella, M., opp, U., Saglia, R. P., Bender, R., Drory, N., Salvato, M., Gabasch, A., & Feulner, G. 2006, *ApJ*, 639, L1
- Papovich, C., et al. 2004, *ApJS*, 154, 70
- Peng, C. Y. 2007, *ApJ*, 671, 1098
- Peng, C. Y., Impey, C. D., Ho, L. C., Barton, E., & Rix, H.-W. 2006, *ApJ*, 640, 114
- Pérez-González, P. G., et al. 2005, *ApJ*, 630, 82
- Pierce, C. M., et al. 2007, *ApJ*, 660, L19
- Pounds, K. A., Reeves, J. N., King, A. R., Page, K. L., O'Brien, P. T., & Turner, M. J. L. 2003, *MNRAS*, 345, 705
- Rafferty, D. A., McNamara, B. R., Nulsen, P. E. J., & Wise, M. W. 2006, *ApJ*, 652, 216
- Reddy, N. A., Steidel, C. C., Pettini, M., Adelberger, K. L., Shapley, A. E., Erb, D. K., & Dickinson, M. 2008, *ApJS*, 175, 48
- Renzini, A. 2006, *ARA&A*, 44, 141
- Richards, G. T., et al. 2006a, *ApJS*, 166, 470
- Richards, G. T., et al. 2006b, *AJ*, 131, 2766
- Rieke, G. H., et al. 2004, *ApJS*, 154, 25
- Rieke, G. H., Alonso-Herrero, A., Weiner, B. J., Pérez-González, P. G., Blaylock, M., Donley, J. L., & Marcillac, D. 2009, *ApJ*, 692, 556
- Rix, H.-W., et al. 2004, *ApJS*, 152, 163
- Robaina, A. R., et al. 2009, *ApJ*, submitted
- Robertson, B., Cox, T. J., Hernquist, L., Franx, M., Hopkins, P. F., Martini, P., Springel, V. 2006, *ApJ*, 641, 21
- Robertson, B., Hernquist, L., Cox, T. J., Di Matteo, T., Hopkins, P. F., Martini, P., & Springel, V. 2006, *ApJ*, 641, 90
- Rudnick, G., et al. 2006, *ApJ*, 650, 624
- Sanders, D. B., Mazzarella, J. M., Kim, D.-C., Surace, J. A., & Soifer, B. T. 2003, *AJ*, 126, 1607
- Schimminovich, D., et al. 2005, *ApJ*, 619, L47
- Schimminovich, D., et al. 2007, *ApJS*, 173, 315
- Seymour, N., et al. 2008, *MNRAS*, 386, 1695
- Shankar, F., Salucci, P., Granato, G. L., De Zotti, G., & Danese, L. 2004, *MNRAS*, 354, 1020
- Shi, Y., Rieke, G., Lotz, J., & Pérez-González, P. G. 2009, *ApJ*, 697, 1764
- Shields, G. A., Menezes, K. L., Massart, C. A., & Vanden Bout, P. 2006, *ApJ*, 641, 683
- Silk, J., & Rees, M. J. 1998, *A&A*, 331, L1
- Silverman, J. D., et al. 2009, *ApJ*, 696, 396
- Smolčić, V., et al. 2009, *ApJ*, 690, 610
- Somerville, R. S., Hopkins, P. F., Cox, T. J., Robertson, B. E., & Hernquist, L. 2008, *MNRAS*, 391, 481

- Thomas, D., Maraston, C., Bender, R., & de Oliveira, C. M. 2005, *ApJ*, 621, 673
- Trager, S. C., Faber, S. M., Worthey, G., & González, J. J. 2000, *AJ*, 120, 165
- Tremonti, C. A., Moustakas, J., & Diamond-Stanic, A. M. 2007, *ApJ*, 663, 77
- Treu, T., Malkan, M. A., & Blandford, R. D. 2004, *ApJ*, 615, L97
- Treu, T., Woo, J.-H., Malkan, M. A., & Blandford, R. D. 2007, *ApJ*, 667, 117
- Ueda, Y., Akiyama, M., Ohta, K., & Miyaji, T., 2003, *ApJ*, 598, 886
- van der Wel, A., Holden, B. P., Zirm, A. W., Franx, M., Rettura, A., Illingworth, G. D., & Ford, H. C. 2008, *ApJ*, 688, 48
- Vestergaard, M., & Peterson, B. M. 2006, *ApJ*, 641, 689
- Wandel, A., Peterson, B. M., & Malkan, M. A. 1999, *ApJ*, 526, 579
- Watson, C. R., et al. 2009, *ApJ*, 696, 2206
- Wilkins, S. M., Trentham, N., & Hopkins, A. M. 2008, *MNRAS*, 385, 687
- Wolf, C., et al. 2004, *A&A*, 421, 913
- Wolf, C., et al. 2005, *ApJ*, 630, 771
- Woo, J.-H., Treu, T., Malkan, M. A., & Blandford, R. D. 2006, *ApJ*, 645, 900
- Wyithe, J. S. B., & Loeb, A. 2003, *ApJ*, 595, 614
- Younger, J. D., Hopkins, P. F., Cox, T. J., & Hernquist, L. 2008, *ApJ*, 686, 815
- Yu, Q., & Tremaine, S. 2002, *MNRAS*, 335, 965
- Zheng, X. Z., Bell, E. F., Rix, H.-W., Papovich, C., Le Floch, E., Rieke, G. H., & Pérez-González, P. G. 2006, *ApJ*, 640, 784
- Zheng, X. Z., Dole, H., Bell, E. F., Le Floch, E., Rieke, G. H., Rix, H.-W., & Schiminovich, D. 2007, *ApJ*, 670, 301